

Test particle motion in the space–time of a Kerr black hole pierced by a cosmic string

Eva Hackmann ^{(a),*} Betti Hartmann ^{(b),†} Claus Lämmerzahl ^{(a),(c),‡} and Parinya Sirimachan ^{(b),§}

^(a) ZARM, Universität Bremen, Am Fallturm, 28359 Bremen, Germany

^(b) School of Engineering and Science, Jacobs University Bremen, 28759 Bremen, Germany

^(c) Institut für Physik, Universität Oldenburg, 26111 Oldenburg, Germany

(Dated: August 22, 2018)

We study the geodesic equation in the space-time of a Kerr black hole pierced by an infinitely thin cosmic string and give the complete set of analytical solutions of this equation for massive and massless particles in terms of Mino time that allows to decouple the r - and θ -component of the geodesic equation. The solutions of the geodesic equation can be classified according to the particle's energy and angular momentum, the mass and angular momentum per mass of the black hole. We give examples of orbits showing the influence of the cosmic string. We also discuss the perihelion shift and the Lense-Thirring effect for bound orbits and show that the presence of a cosmic string enhances both effects. Comparing our results with experimental data from the LAGEOS satellites we find an upper bound on the energy per unit length of a string piercing the earth which is approximately 10^{16} kg/m. Our work has also applications to the recently suggested explanation of the alignment of the polarization vector of quasars using remnants of cosmic string decay in the form of primordial magnetic field loops.

PACS numbers: 04.20.Jb, 02.30.Hq

I. INTRODUCTION

The motion of test particles (both massive and massless) provides the only experimentally feasible way to study the gravitational fields of objects such as black holes. Predictions about observable effects (light-like deflection, gravitational time-delay, perihelion shift and Lense-Thirring effect) can be made and compared with observations. Geodesics in black hole space-times in 4 dimensional Schwarzschild space-time [1] and Kerr and Kerr–Newman space-time [2] have been discussed extensively. This has been extended to the cases of Schwarzschild–de Sitter space-times [3] as well as to spherically symmetric higher dimensional space-times [4]. The analytical solutions of the geodesic equation in the Kerr space-time have been presented in [2, 5]. Moreover, solutions of the geodesic equation in the Kerr space-time have been given using elliptic functions [6], while solutions representing bound orbits parameterized in terms of *Mino time* [7] have been presented in [8]. Spherical orbits in the Kerr–(Anti)–de Sitter space-time have been discussed in [6], while the general solution to the geodesic equation in (4-dimensional) Kerr–de Sitter [9] and even general Plebanski–Demianski space-times without acceleration has been found [10].

In [11] a Fourier expansion has been used to compute the fundamental frequencies for bound orbits using Mino time. These results have direct application in the computation of gravitational waves that are created in extreme mass ratio inspirals, i.e. in binaries in which a stellar object moves on a bound orbit around a supermassive black hole.

Cosmic strings have gained a lot of renewed interest over the past years due to their possible connection to string theory [12]. These are topological defects [13] that could have formed in one of the numerous phase transitions in the early universe due to the Kibble mechanism. Inflationary models resulting from string theory (e.g. brane inflation) predict the formation of cosmic string networks at the end of inflation [14].

Different space-times containing cosmic strings have been discussed in the past. This study has mainly been motivated by the pioneering work of Bach and Weyl [15] describing a pair of black holes held apart by an infinitely thin strut. This solution has later been reinterpreted in terms of cosmic strings describing a pair of black holes held apart by two cosmic strings extending to infinity in opposite direction. Consequently, a cosmic string piercing a Schwarzschild black hole has also been discussed, both in the thin string limit [16] – where an analytic solution can be given – as well as using the full U(1) Abelian-Higgs model [17, 18], where only numerical solutions are available. In the latter case, these solutions have been interpreted to represent black hole solutions with long range “hair” and

*Electronic address: hackmann@zarm.uni-bremen.de

†Electronic address: b.hartmann@jacobs-university.de

‡Electronic address: laemmerzahl@zarm.uni-bremen.de

§Electronic address: p.sirimachan@jacobs-university.de

are thus counterexamples to the No hair conjecture which states that black holes are uniquely characterized by their mass, charge and angular momentum. Interestingly, the solution found in [16] is a Schwarzschild solution which however differs from the standard spherically symmetric case by the replacement of the angular variable ϕ by $\beta\phi$, where the parameter β is related to the deficit angle by $\delta = 2\pi(1 - \beta)$. In this sense, the space-time is thus not uniquely determined by the mass, but is described by the mass *and* deficit angle parameter β . Of course, it is then easy to extend known analytically given space-times to the conical case by making the mentioned substitution.

In order to understand details of gravitational fields of massive objects and to be able to predict observational consequences, it is important to understand how test particles move in these space-times. Next to the above mentioned examples the complete set of solutions to the geodesic equation in the space-time of a Schwarzschild black hole pierced by a cosmic string has been given recently in [19].

The geodesic equation for the motion of test particles in the space-time of an uncharged, rotating black hole in 4 space-time dimensions (given by the Kerr solution) pierced by an infinitely thin string aligned with the rotation axis of the black hole has been given in [20] and spherical orbits and the Lense–Thirring precession have been discussed. Solutions to the geodesic equation in this space-time have also been given in [21], but the test particle motion has been restricted to the equatorial plane and gravitomagnetic effects have been studied. Moreover, small perturbations around circular orbits have been discussed in [22]. The motion of a test scalar quantum particle in the space-time of a Kerr–Newman black hole pierced by a cosmic string has been discussed in [23] and it was observed that the presence of a cosmic string alters the corresponding observables.

The aim of this paper is to determine the *complete set* of analytic solutions of the geodesic equations in the space-time of a Kerr black hole pierced by a cosmic string and to derive analytical expressions for observable effects which can be used for astrophysical searches for such cosmic strings. The accurate computation of geodesics for massive particles is important in order to understand gravitational wave signals from binaries which can later be compared with eventual gravitational wave measurements. The computation of geodesics for massless particles is important in order to understand how light signals pass by black holes or other massive objects. Moreover, our work has a direct link to the recently proposed explanation [24] of the observed alignment of the polarization vector of quasars on cosmological scales [25]. In [24] the assumption is used that two originally linked electroweak string loops decayed via the formation of monopole–antimonopole pairs in the early universe. The remnants of this decay are interconnected loops of magnetic field whose radii have grown due to the expansion of the universe and today should be on the order of Gpc. Interestingly, it was found that the rotation axis of a quasar would align with the direction of the magnetic field. Since the size of the magnetic field loops are much larger than the size of the quasars, we can assume the loop to be approximated by a straight line of magnetic field – that is aligned with the rotation axis of the supermassive black hole in the center of the quasar – at the position of the quasar. If we assume our infinitely thin cosmic string to be a toy model for finite width strings (e.g. electroweak or Abelian–Higgs strings) where the latter would have a magnetic flux along their axis, the model studied in this paper would describe a quasar with its rotation axis equal to the axis of the magnetic flux.

Our paper is organized as follows: in Section II, we give the geodesic equation, in Section III, we classify the solutions, while in Section IV, we give the solutions to the geodesic equation and in Section V we present examples of orbits. In Section VI we discuss observables such as the perihelion shift and the Lense–Thirring effect. We conclude in Section VII.

II. THE GEODESIC EQUATION

We consider the geodesic equation

$$\frac{d^2 x^\mu}{d\tau^2} + \Gamma_{\rho\sigma}^\mu \frac{dx^\rho}{d\tau} \frac{dx^\sigma}{d\tau} = 0, \quad (1)$$

where $\Gamma_{\rho\sigma}^\mu$ denotes the Christoffel symbol given by

$$\Gamma_{\rho\sigma}^\mu = \frac{1}{2} g^{\mu\nu} (\partial_\rho g_{\sigma\nu} + \partial_\sigma g_{\rho\nu} - \partial_\nu g_{\rho\sigma}) \quad (2)$$

and τ is an affine parameter such that for time-like geodesics $d\tau^2 = g_{\mu\nu} dx^\mu dx^\nu$ corresponds to proper time.

The explicit form of the metric that we are studying in this paper reads

$$ds^2 = - \left(1 - \frac{2Mr}{\rho^2} \right) dt^2 + \frac{\rho^2}{\Delta} dr^2 + \rho^2 d\theta^2 + \beta^2 \left(r^2 + a^2 + \frac{2Mra^2 \sin^2 \theta}{\rho^2} \right) \sin^2 \theta d\phi^2 - \beta \frac{4Mra \sin^2 \theta}{\rho^2} dt d\phi, \quad (3)$$

where $\rho^2 = r^2 + a^2 \cos^2 \theta$, $\Delta = r^2 - 2Mr + a^2$, $a = J/M$ is the angular momentum J per mass M of the black hole and $0 < \beta < 1$ is the deficit angle parameter that is related to the deficit angle $\delta = 2\pi(1 - \beta)$. This metric describes a Kerr black hole pierced by an infinitely thin cosmic string that is aligned with the rotation axis of the black hole. The deficit angle appears due to the presence of the cosmic string and can be expressed in terms of the energy per unit length μ of the cosmic string : $\delta = 8\pi G\mu \sim 8\pi(\eta/M_{\text{Pl}})^2$, where η is the typical symmetry breaking scale at which the cosmic string formed and M_{Pl} is the Planck mass. Note that we are using units such that $G = c = 1$.

For $a = 0$ this metric reduces to the Schwarzschild solution pierced by an infinitely thin cosmic string [19], while for $\beta = 1$ we recover the standard Kerr solution.

Surfaces with $\Delta = 0$ correspond to horizons of the Kerr solution with horizon radius $r_{\pm} = M \pm \sqrt{M^2 - a^2}$, where the + sign corresponds to the event horizon, while the - sign corresponds to the Cauchy horizon. Surfaces with $2Mr = \rho^2$ are the static limit and define a Killing horizon. The domain between the event horizon and the static limit is the ergosphere. In the following, we are only interested in non-extremal black hole solutions, i.e. in solutions with $M^2 > a^2$. Note that the localization of the horizons and the static limit, respectively are not altered by the presence of the cosmic string.

The Boyer-Lindquist coordinates (r, θ, ϕ) are related to cartesian coordinate (x, y, z) by $x = \sqrt{r^2 + a^2} \sin \theta \cos(\beta\phi)$, $y = \sqrt{r^2 + a^2} \sin \theta \sin(\beta\phi)$ and $z = r \cos \theta$. Hence $r = 0$ corresponds to a disc with a deficit angle δ , while the physical singularity at $r = 0$, $\theta = \pi/2$ is a ring with a deficit angle. It is then clear - in contrast to the $a = 0$ limit - that negative values of r are allowed. When crossing $r = 0$ to negative values of r one enters into another conical space-time that however possesses no horizons. The Penrose diagram of this space-time looks exactly like that of the standard Kerr space-time [5], however each point in the diagram would correspond to a sphere with deficit angle δ .

The Lagrangian reads

$$\mathcal{L} = \frac{1}{2} g_{\mu\nu} \frac{dx^\mu}{d\tau} \frac{dx^\nu}{d\tau} = \frac{1}{2} \varepsilon, \quad (4)$$

where $\varepsilon = -1$ for massive test particles and $\varepsilon = 0$ for massless test particles, respectively. The Killing vectors of this space-time are $\frac{\partial}{\partial t}$ and $\frac{\partial}{\partial \phi}$. The constants of motion are the energy E and the angular momentum L_z which are given by the generalized momenta p_t and p_ϕ

$$-p_t = -\frac{\partial \mathcal{L}}{\partial \dot{t}} = -\dot{t} g_{tt} - \dot{\phi} g_{t\phi} = \left(1 - \frac{2Mr}{\rho^2}\right) \dot{t} + \beta \frac{2Mar}{\rho^2} \sin^2 \theta \dot{\phi} =: E, \quad (5)$$

$$p_\phi = \frac{\partial \mathcal{L}}{\partial \dot{\phi}} = \dot{t} g_{t\phi} + \dot{\phi} g_{\phi\phi} = -\beta \frac{2Mar}{\rho^2} \sin^2 \theta \dot{t} + \beta^2 \frac{(r^2 + a^2)^2 - \Delta a^2 \sin^2 \theta}{\rho^2} \sin^2 \theta \dot{\phi} =: \beta L_z. \quad (6)$$

The dot denotes the differentiation with respect to the affine parameter τ . Therefore the presence of a cosmic string aligned with the rotation axis of the Kerr black hole decreases the magnitude of the generalized momenta due to the parameter β as compared to the standard Kerr space-time. In particular, for a given energy E a particle on the surface defined by $g_{tt} = 0$ (the static limit) has larger $\dot{\phi}$ as compared to the standard Kerr case.

There is another constant of motion, namely the Carter constant K [26] that appears when separating the Hamilton-Jacobi equations

$$\frac{\partial S}{\partial \tau} = \frac{1}{2} g^{\mu\nu} (\partial_\mu S) (\partial_\nu S), \quad (7)$$

which persists in the presence of a cosmic string. S denotes the principal function of Hamilton for which we make the following Ansatz

$$S = \frac{1}{2} \varepsilon \tau - Et + \beta L_z \phi + S_r(r) + S_\theta(\theta), \quad (8)$$

where $S_r(r)$ and $S_\theta(\theta)$ are functions of r and θ only, respectively.

By differentiating S with respect to the constants ε , E , L_z and $\mathcal{Q} := K - (L_z - aE)^2$, where \mathcal{Q} is the modified Carter constant, we find the geodesic equations

$$\rho^2 \dot{r} = \pm \sqrt{R(r)}, \quad (9)$$

$$\rho^2 \dot{\theta} = \pm \sqrt{\Theta(\theta)}, \quad (10)$$

$$\rho^2 \beta \dot{\phi} = (L_z \csc^2 \theta - aE) + \frac{aP(r)}{\Delta(r)}, \quad (11)$$

$$\rho^2 \dot{t} = a(L_z - aE \sin^2 \theta) + \frac{(r^2 + a^2)P(r)}{\Delta(r)} \quad (12)$$

with

$$\Theta(\theta) = \mathcal{Q} - \cos^2 \theta (L_z^2 \csc^2 \theta - a^2(E^2 + \varepsilon)) \quad , \quad (13)$$

$$P(r) = E(r^2 + a^2) - L_z a \quad , \quad (14)$$

$$R(r) = P(r)^2 - \Delta(r) (\mathcal{Q} + (L_z - aE)^2 - \varepsilon r^2) \quad . \quad (15)$$

Introducing a new parameter, the so-called *Mino time* [7] given by $d\lambda = \frac{dr}{\rho^2}$ the r - and θ -component of the geodesic equation can be decoupled

$$\frac{dr}{d\lambda} = \pm \sqrt{R(r)} \quad , \quad (16)$$

$$\frac{d\theta}{d\lambda} = \pm \sqrt{\Theta(\theta)} \quad , \quad (17)$$

$$\frac{d\phi}{d\lambda} = \frac{1}{\beta} \left(\frac{L_z \csc^2 \theta - aE}{\sqrt{\Theta(\theta)}} \frac{d\theta}{d\lambda} + \frac{aP(r)}{\Delta(r)\sqrt{R(r)}} \frac{dr}{d\lambda} \right) \quad , \quad (18)$$

$$\frac{dt}{d\lambda} = \frac{a(L_z - aE \sin^2 \theta)}{\sqrt{\Theta(\theta)}} \frac{d\theta}{d\lambda} + \frac{(r^2 + a^2)P(r)}{\Delta(r)\sqrt{R(r)}} \frac{dr}{d\lambda} \quad . \quad (19)$$

For $a = 0$ these equations reduce to the equations of motion in a space-time of a Schwarzschild black hole pierced by a cosmic string [19], while for $\beta = 1$ we recover the geodesic equation in the Kerr space-time. As initial conditions we will choose the $+$ -signs in (16) and (17).

III. CLASSIFICATION OF SOLUTIONS

The classification of the solutions of the geodesic equations (16)-(19) can be done with respect to the modified Carter constant \mathcal{Q} , the mass of the black hole M , the angular momentum per unit mass of the black hole a as well as the energy E and angular momentum L_z of the massive ($\varepsilon = -1$) or massless ($\varepsilon = 0$) test particle. Apparently, the deficit parameter β does not appear in the r , θ and t component of the geodesic equation and will hence only influence the ϕ -motion.

A. r -motion

In order to have solutions of the geodesic equation for r we have to require $R(r) > 0$. Therefore solutions of the r -component of the geodesic equation exist only for specific choices of E and L_z . $R(r)$ will have either 4 real, 2 real and 2 complex or 4 complex zeros. On the boundaries between the domains in the E^2 - L_z -plane corresponding to these three different possibilities $R(r)$ necessarily has a double zero. In order to find these boundaries we make the Ansatz $R(r) = (r - \kappa)^2 ((E^2 + \varepsilon)r^2 + \rho_1 r + \rho_2)$ where κ , ρ_1 and ρ_2 have to be determined. We find that for $R(r) = 0$ we have the following parametric expressions for E and L_z

$$E(\kappa) = \frac{-2\kappa^3 - 3\varepsilon M \kappa^2 + (\varepsilon a^2)\kappa - KM}{\sqrt{P_\kappa}} \quad , \quad (20)$$

$$L_z(\kappa) = \frac{\varepsilon M \kappa^4 + (K - 2a^2 - \varepsilon a^2)\kappa^3 - (3MK + 3\varepsilon M a^2)\kappa^2 + (\varepsilon a^4 + a^2 K)\kappa + a^2 MK}{a\sqrt{P_\kappa}} \quad , \quad (21)$$

where

$$P_\kappa = 4\kappa^6 + 8\varepsilon M \kappa^5 + (4K - 4a\varepsilon)\kappa^4 - 8MK \kappa^3 + 4a^2 K \kappa^2 \quad . \quad (22)$$

Note that $r = \kappa$ corresponds to a double zero of $R(r)$ and hence represents spherical orbits.

Examples for the polynomial $R(r)$ are given in Fig.1 and Fig 2. In Fig.1 we show the different domains in the E^2 - L_z -plane for $M = 1$, $a = 0.8$ and $K = 4$. The blue line corresponds to $E^2 = 1$, the green line to $\kappa \in] - \infty, 0]$ and the red line to $\kappa \in [0, +\infty[$. The plots of $R(r)$ in the domains R1 to R5 are also shown. For R1 $R(r)$ possesses 4 complex zeros, for R2 and R5 2 real and 2 complex zeros, while for R3 and R4 there are four real zeros. The following type of orbits are then possible [5] :

- **Flyby orbit:** the test particle starts from $\pm\infty$, reaches a minimal value of $|r|$ and flies back to $r = \pm\infty$. There are two flyby orbits in R2 and R4, respectively.
- **Transit orbit:** the test particle starts from $\pm\infty$, crosses $r = 0$ and continues to $r = \mp\infty$. There is a transit orbit in R1.
- **Bound orbit:** the test particle oscillates in an interval $[r_2, r_1]$ where $r_1 > r_2$. There are two bound orbits in R3 and one bound orbit in R4 and R5, respectively.
- **Spherical orbit:** this is a special bound orbit with r constant. $r = \kappa$ is a spherical orbit that can be stable or unstable.

In Fig.2 we show how the domains R1 to R5 change when changing the Carter constant K (upper three figures). Obviously R3 decreases in size when increasing K . We also give the change of R1 to R5 for changing angular momentum per unit mass a (lower three figures). In this case, the domain R4 is increasing for increasing a .

B. θ -motion

It is obvious from the form of the geodesic equations that we should have $\Theta(\theta) > 0$, i.e. θ -motion is allowed only for those θ for which $\Theta(\theta) > 0$. This in turn means that when we fix \mathcal{Q} and a only particular values of E and L_z are allowed.

1. equatorial motion with $\theta = \pi/2$ for massive and massless particles: in this case, it follows from (13) that $\mathcal{Q} = 0$, i.e.

$$L_z = aE \pm \sqrt{K}. \quad (23)$$

This is shown in Fig.3(a) and Fig.3(b) where the blue and the red line indicate $L_z = aE + \sqrt{K}$ and $L_z = aE - \sqrt{K}$, respectively.

2. polar motion with $\theta = 0$ or $\theta = \pi$: obviously in this case, we have to choose $L_z = 0$ and $\mathcal{Q} \geq -a^2(E^2 + \varepsilon)$.
3. motion for $0 < \theta < \pi$ with $\theta \neq \pi/2$: in this case, we find that (see Appendix for details)

$$L_z \geq \frac{1}{2} \frac{(E - \sqrt{E^2 - \varepsilon})(a^2\varepsilon + K)}{\varepsilon a} \quad (24)$$

for massive particles and

$$L_z \geq \frac{K}{4aE^2} \quad (25)$$

for massless particles. This is shown in Fig.3(a) and Fig.3(b) where the green line indicates $L_z = \frac{1}{2} (E - \sqrt{E^2 - \varepsilon})(a^2\varepsilon + K)/(\varepsilon a)$. The allowed domain in the L_z - E^2 -plane is the one above this green line.

We show an example of the different domains corresponding to zeros of $\Theta(\theta)$ in Fig.4 for $M = 1$, $a = 0.8$ and $K = 4$. The function $\Theta(\theta)$ is plotted for the domains denoted $T1$ to $T5$. In domains $T1$, $T2$ and $T5$ the polynomial $\Theta(\theta)$ has no real zeros, while it has four real zeros in domain $T3$ and two real zeros in domain $T4$, respectively. Clearly, only in the domains $T3$ and $T4$ solutions to the geodesic equations exist. In $T3$ there are two domains in θ for which $\Theta(\theta) > 0$. Here the particles oscillate between θ_{\min} and θ_{\max} but cannot cross $\theta = \frac{\pi}{2}$. In domain $T4$ the particle can cross the equatorial plane $\theta = \pi/2$.

IV. ANALYTICAL SOLUTIONS OF THE GEODESIC EQUATION

In the following, we will present the analytical solutions of the geodesic equation for the r , θ , ϕ and t component. We will present these solutions using Mino time λ .

A. r -motion

The polynomial $R(r)$ can be written in the form

$$R(r) = (E^2 + \varepsilon) \prod_{j=1}^4 (r - r_j), \quad (26)$$

where the r_j denote the zeros of $R(r)$ with r_1 the largest real zero. Using the coordinate transformation $r = 1/y + r_1$ the polynomial $R(r)$ can be transformed to a 3rd order polynomial in y using

$$d\lambda = \frac{dr}{\sqrt{R(r)}} = -\frac{dy}{\sqrt{(E^2 + \varepsilon) \sum_{i=0}^3 b_i y^i}} \quad (27)$$

with

$$b_0 = 1, \quad (28)$$

$$b_1 = (-r_2 - r_4 + 3r_1 - r_3), \quad (29)$$

$$b_2 = (r_2 r_4 - 2r_1 r_2 + r_2 r_3 + 3r_1^2 - 2r_1 r_3 - 2r_1 r_4 + r_3 r_4), \quad (30)$$

$$b_3 = (-r_3 r_1^2 + r_1 r_2 r_3 + r_1 r_2 r_4 + r_1 r_3 r_4 - r_2 r_1^2 + r_1^3 - r_4 r_1^2 - r_2 r_3 r_4). \quad (31)$$

Introducing the variable

$$z = \frac{y - \alpha}{\gamma} \quad \text{with} \quad \gamma = \sqrt[3]{\frac{4}{b_3(E^2 + \varepsilon)}}, \quad \alpha = -\frac{b_2}{3b_3} \quad (32)$$

we can write the solution of (16) as follows :

$$r(\lambda) = \left(\frac{1}{\gamma \wp\left(\frac{1}{\gamma}(\lambda - \lambda_0) + C_r; \tilde{g}_2, \tilde{g}_3\right) + \alpha} + r_1 \right). \quad (33)$$

The integration constant is given by

$$C_r = \int_{z_0}^{\infty} \frac{dz}{\sqrt{4z^3 - \tilde{g}_2 z - \tilde{g}_3}}, \quad (34)$$

where z_0 denotes the value of z that corresponds to the initial radius and

$$\tilde{g}_2 = -\frac{2^{2/3} \sqrt[3]{(E^2 + \varepsilon)^2 b_3^2 (-b_2^2 + 3b_1 b_3)}}{3b_3^2}, \quad \tilde{g}_3 = -\frac{(E^2 + \varepsilon)(2b_2^3 + 27b_0 b_3^2 - 9b_1 b_2 b_3)}{27b_3^2}. \quad (35)$$

Depending on the sign of the discriminant $\tilde{D} = \tilde{g}_2^3 - 27\tilde{g}_3^2$ we have different values for C_r . In the following, we will denote the zeros of the 3rd order polynomial in the square zero of (34) as $\tilde{e}_1 > \tilde{e}_2 > \tilde{e}_3$.

1. $\tilde{D} > 0$: In this case $R(r)$ has four real zeros which corresponds to domains R3 and R4 in Fig.1.

For the outer bound orbit in domain R3 with minimal radius r_2 and maximal radius r_1 we choose $z_0 = \tilde{e}_1$ such that $C_r = K(\mathcal{K})/\sqrt{\tilde{e}_1 - \tilde{e}_3} =: \tilde{\omega}_1$ where $K(\mathcal{K})$ is the complete elliptic integral of the first kind and $\mathcal{K} = \sqrt{\tilde{e}_2 - \tilde{e}_3}/\sqrt{\tilde{e}_1 - \tilde{e}_3}$ is the modulus of the elliptic integral. For the inner bound orbit in domain R3 with minimal radius r_4 and maximal radius r_3 we choose $z_0 = \tilde{e}_2$ such that $C_r = K(\mathcal{K})/\sqrt{\tilde{e}_1 - \tilde{e}_3} + iK(\mathcal{K}')/\sqrt{\tilde{e}_1 - \tilde{e}_3} =: \tilde{\omega}_1 + \tilde{\omega}_2$ where $\mathcal{K}' = \sqrt{1 - \mathcal{K}^2}$. For the flyby orbit in R4 with initial minimal radius r_1 , we choose $z_0 = \infty$ such that $C_r = 0$, while for the inner bound orbit in R4 with initial maximal radius r_2 and minimal radius r_3 we choose $z_0 = \tilde{e}_2$ such that $C_r = \tilde{\omega}_1 + \tilde{\omega}_2$.

2. $\tilde{D} < 0$: In this case $R(r)$ has two real zeros which corresponds to domains R2 and R5 in Fig.1. In the following, we will denote the real zero of the 3rd order polynomial in the square zero of (34) as \tilde{e}_2 , while the two complex zeros are denoted by \tilde{e}_1 and \tilde{e}_3 .

For the flyby orbit in domain R2 with initial minimal radius r_1 we choose $z_0 = \infty$ such that $C_r = 0$. For the bound orbit in domain R5 with initial maximal radius r_1 we also choose $z_0 = \infty$, i.e. $C_r = 0$.

3. $\tilde{D} = 0$: In this case $R(r)$ has one real zero. The orbit in this case will be a bound spherical orbit.

Note that there is also the possibility of four complex zeros. This however would simply correspond to a transit orbit with $r = -\infty \rightarrow +\infty$. We will not discuss this case in detail in this paper.

B. θ -motion

The solution of (17) as a function of Mino time λ is given by

$$\theta(\lambda) = \arccos \left[\pm \frac{1}{\sqrt{\mu \wp \left(\frac{1}{\mu}(\lambda - \lambda_0) + C_\theta; g_2, g_3 \right) + \nu}} \right], \quad (36)$$

where

$$\mu = \mathcal{Q}^{-1/3}, \quad \nu = (\mathcal{Q} + L_z^2 - a^2(E^2 + \varepsilon)) / (3\mathcal{Q}). \quad (37)$$

The positive (negative) sign of the arccos corresponds to the choice $\theta > \pi/2$ ($\theta < \pi/2$). For the θ motion in domain T4, the solutions thus have to be “glued together” at $\theta = \pi/2$.

The integration constant C_θ is given by

$$C_\theta = \int_{w_0}^{\infty} \frac{dw}{\sqrt{4w^3 - g_2w - g_3}}, \quad (38)$$

where w is related to θ by $\cos^2 \theta = (\mu w + \nu)^{-1}$, w_0 corresponds to the value of w that represents the initial θ and

$$g_2 = -\frac{2^{2/3}(a_1^2)^{1/3}(3a_1a_3 - a_2^2)}{3a_1^2}, \quad g_3 = -\frac{2a_2^3 - 9a_1a_2a_3}{27a_1^2}, \quad (39)$$

where $a_1 = 4\mathcal{Q}$, $a_2 = 4(a^2(E^2 + \varepsilon) - L_z - \mathcal{Q})$ and $a_3 = -4a^2(E^2 + \varepsilon)$. The discriminant $D = g_2^3 - 27g_3^2$ is always positive, so we have three real zeros of the 3rd order polynomial, which we call $e_1 > e_2 > e_3$ in the following. Note that though we might have three real zeros for the polynomial in w these zeros might not fulfill $(\mu w + \nu)^{-1} = \cos^2 \theta \leq 1$. Moreover to each zero of the polynomial in w correspond two values of θ fulfilling $\cos \theta = \pm(\mu w + \nu)^{-1/2}$. Hence, depending on the values of e_1 , e_2 and e_3 the polynomial $\Theta(\theta)$ can have four, two or no real zeros.

In T4, we typically choose $w_0 = e_1$ such that $C_\theta = K(\mathcal{K})/\sqrt{e_1 - e_3} =: \omega_1$, where $K(\mathcal{K})$ is the complete elliptic integral of the first kind and $\mathcal{K} = \sqrt{e_2 - e_3}/\sqrt{e_1 - e_3}$ is the modulus of the elliptic integral.

In T3, we typically choose $w_0 = e_3$ such that $C_\theta = iK(\mathcal{K}')/\sqrt{e_1 - e_3} =: \omega_2$, where $K(\mathcal{K}') = \sqrt{1 - \mathcal{K}^2}$.

C. ϕ -motion

The equation for the ϕ component (18) is separated into a θ -dependent and r -dependent part

$$\beta d\phi = \frac{L_z \csc^2 \theta - aE}{\sqrt{\Theta(\theta)}} d\theta + \frac{a\Delta^{-1}P(r)}{\sqrt{R(r)}} dr =: dI_\theta + dI_r. \quad (40)$$

The solutions for I_θ and I_r are (see Appendix for more details) :

$$I_\theta = (L_z - aE)(\lambda - \lambda_0) + \sum_{i=1}^2 \frac{\nu + \mu d_0}{\wp'(x_i)} \left[\frac{(\lambda - \lambda_0)}{\mu} \zeta(x_i) + \ln(\sigma(x - x_i)) - \ln(\sigma(x_0 - x_i)) \right], \quad (41)$$

$$I_r = -K_0(\lambda - \lambda_0) + \sum_{i,j=1}^2 \frac{K_j}{\wp'(u_{ji})} \left[\frac{-(\lambda - \lambda_0)}{\gamma} \zeta(u_{ji}) + \ln(\sigma(u - u_{ji})) - \ln(\sigma(u_0 - u_{ji})) \right], \quad (42)$$

where ζ and σ denote the Weierstrass zeta- and sigma-function, respectively. μ and ν are the variables defined in (37), $d_0 = (1 - \nu)/\mu$ and $x = \lambda/\mu$. Moreover, we have introduced the variable $u = -\left(\frac{1}{\gamma}(\lambda - \lambda_0) + C_r\right)$ with $u(\lambda_0) = -C_r$ and the γ given in (32). In addition $u_{ji} = e_j$ with $\wp(u_{11}) = \wp(u_{12}) = e_1$ and $\wp(u_{21}) = \wp(u_{22}) = e_2$. Finally, the K_j appear when rewriting dI_r as follows

$$dI_r = K_0 \frac{\gamma dz}{\sqrt{4z^3 - \tilde{g}_2 z - \tilde{g}_3}} + \sum_{j=1}^2 K_j \frac{dz}{(z - e_j) \sqrt{4z^3 - \tilde{g}_2 z - \tilde{g}_3}}, \quad (43)$$

where $e_j := \frac{y_j - \alpha}{\gamma}$ and $y = (r - r_1)^{-1}$.

D. t -motion

From (19) we have

$$dt = a(L_z - aE \sin^2 \theta) \frac{d\theta}{\sqrt{\Theta(\theta)}} + (r^2 + a^2)\Delta(r)^{-1}P(r) \frac{dr}{\sqrt{R(r)}} =: d\bar{I}_\theta + d\bar{I}_r. \quad (44)$$

To find analytical expressions for \bar{I}_θ and \bar{I}_r we proceed as in the case of I_θ and I_r , respectively (see also Appendix) and find

$$\bar{I}_\theta = a(L_z - aE)(\lambda - \lambda_0) + a^2 E \sum_{i=1}^2 \frac{1}{\wp'(\bar{x}_i)} \left[\frac{(\lambda - \lambda_0)}{\mu} \zeta(\bar{x}_i) + \ln(\sigma(x - \bar{x}_i)) - \ln(\sigma(x_0 - \bar{x}_i)) \right], \quad (45)$$

where $\wp(\bar{x}_1) = \wp(\bar{x}_2) = -\nu/\mu$. The simple poles of the function (63) given by \bar{x}_1, \bar{x}_2 are in the fundamental domain $\{2a\omega_1 + 2b\omega_2 | a, b \in [0, 1]\}$ where $2\omega_1 \in \mathbb{R}$ and $2\omega_2 \in \mathbb{C}$. In addition, we have

$$\bar{I}_r = C_0(\lambda - \lambda_0) + \sum_{i=1}^4 \sum_{j=1}^2 \frac{C_i}{\wp'(u_{ji})} \left[\frac{-(\lambda - \lambda_0)}{\gamma} \zeta(u_{ji}) + \ln(\sigma(u - u_{ji})) - \ln(\sigma(u_0 - u_{ji})) \right], \quad (46)$$

where C_i are the coefficients from the partial fraction and \tilde{e}_i the poles of the rational function $F(z)$ from the transformation $(r^2 + a^2)\Delta(r)^{-1}P(r) \frac{dr}{\sqrt{R(r)}}$. In addition $\wp(u_{1i}) = \wp(u_{2i}) = \tilde{e}_i$.

V. EXAMPLES OF ORBITS

In the following we give plots of geodesics of massive and massless particles, respectively in the space-time of a non-extremal Kerr black hole pierced by an infinitely thin cosmic string. In particular we will demonstrate how the presence of the cosmic string alters the test particle motion.

A. Motion of massive test particles

The domain of existence of solutions of the geodesic equation can be obtained from the intersection of the allowed domains of the L_z - E^2 -plane obtained from the requirement $\Theta(\theta) > 0$ and $R(r) > 0$, respectively. This leads to four domains in the L_z - E^2 -plane. These are shown for $M = 1$, $a = 0.8$ and $K = 12$ in Fig.5 and denoted by Z1 to Z4.

1. **Z1:** This domain is the combination of domain $T4$ from Fig.4 and domain $R3$ from Fig.1. The possible orbits are two bound orbits on which the test particle can cross the equatorial plane at $\theta = \pi/2$. The effect of the cosmic string on the geodesic motion on the outer bound and inner bound orbit is shown in Fig.6 and Fig.7, respectively. Note that the test particle on the inner bound orbit (see Fig.7) crosses the event and the Cauchy horizon (red circles) several times.
2. **Z2:** This domain is the combination of domain $T4$ from Fig.4 and domain $R4$ from Fig.1. The possible orbits are one flyby and one bound orbit on which the test particle can cross the equatorial plane at $\theta = \pi/2$. The effect of the cosmic string on the flyby orbit is shown in Fig.8.
3. **Z3:** This domain is the combination of domain $T4$ from Fig.4 and domain $R2$ from Fig.1.
The possible orbits are two flyby orbits (from r_1 to ∞ and $-\infty$ to r_2) on which the test particle can cross the equatorial plane at $\theta = \pi/2$. The effect of the cosmic string on the flyby orbit (from r_1 to ∞) is shown in Fig.9. Note that the test particle crosses the event and the Cauchy horizon (red circles) several times.
4. **Z4:** This domain is the combination of domain $T4$ from Fig.4 and domain $R5$ from Fig.1.
The possible orbit is one bound orbit on which the test particle can cross the equatorial plane at $\theta = \pi/2$. The effect of the cosmic string on this bound orbit is shown in Fig.10. Note that the test particle crosses the event and the Cauchy horizon (red circles) several times.

B. Motion of massless test particles

The domain of existence of solutions of the geodesic equation can be obtained from the intersection of the allowed domains of the L_z - E^2 -plane obtained from the requirement $\Theta(\theta) > 0$ and $R(r) > 0$, respectively. This leads to three domains in the L_z - E^2 -plane. These are shown for $M = 1$, $a = 0.8$ and $K = 12$ in Fig. 11 and denoted by N1 to N3.

1. **N1**: The possible orbit is a cross-over flyby orbit on which the test particle cannot cross the equatorial plane at $\theta = \pi/2$. The effect of the cosmic string on the cross-over flyby orbit (from r_1 to ∞) is shown in Fig.13
2. **N2**: The possible orbits are one bound and one flyby orbit on which the test particle can cross the equatorial plane at $\theta = \pi/2$. The effect of the cosmic string on the cross-over flyby orbit (from r_1 to ∞) is shown in Fig.8.
3. **N3**: The possible orbits are one flyby and one bound orbit on which the test particle can cross the equatorial plane at $\theta = \pi/2$. The effect of the cosmic string on the flyby and on the bound orbit is shown in Fig.14 and Fig.12, respectively.

VI. OBSERVABLES

For the standard Kerr space-time ($\beta = 1$) the analytical expression of the so-called fundamental frequencies of bound orbits have been given in [11] in the frequency domain using a Fourier transformation and in [8] as a function of a Jacobi elliptic integral. Here, we will present the fundamental frequencies for $\beta \leq 1$ in the form of a Weierstrass elliptic integral \wp and analyze their dependence on the deficit angle.

For bound orbits $r(\lambda)$ and $\theta(\lambda)$ become periodic functions that are independent of each other. We can then define the fundamental frequencies of these bound orbits using Mino time λ . Using the results of Sections IV A and IV B we find

$$\Lambda_r = 2 \int_{r_{\min}}^{r_{\max}} \frac{dr}{\sqrt{R(r)}} = 2\gamma\tilde{\omega}_1, \quad \Lambda_\theta = 4 \int_0^{\cos\theta_{\min}} \frac{d\cos\theta}{\sqrt{\Theta(\cos\theta)}} = 4\mu\omega_1, \quad (47)$$

where $r(\lambda) = r(\lambda + n\Lambda_r)$ and $\theta(\lambda) = \theta(\lambda + n\Lambda_\theta)$ for any integer n [11]. r_{\min} and r_{\max} correspond to the periapsis and the apoapsis in the radial direction, while θ_{\min} corresponds to the minimal value of the polar coordinate. The angular frequencies then read

$$\Upsilon_r = \frac{2\pi}{\Lambda_r} = \frac{\pi}{\gamma\omega_{r1}}, \quad \Upsilon_\theta = \frac{2\pi}{\Lambda_\theta} = \frac{\pi}{2\mu\omega_1}. \quad (48)$$

In [8] the frequencies for the ϕ - and t -component have been defined via an average over the orbital periods Λ_r and Λ_θ . Here we read these periods off from our solutions for the ϕ - and t -component of the geodesic equation. These solutions contain terms that correspond to oscillations with periods Λ_r and Λ_θ , respectively and a term that describes a linear increase in Mino time λ . Υ_ϕ and Γ are the frequencies of ϕ and t in Mino time, respectively that correspond to this linear increase [8]. By using the results of sections IV C and IV D, we can find the expressions for these frequencies. This gives

$$\Upsilon_\phi = \frac{1}{\beta} \left((L_z - aE - K_0) + \sum_{i,j=1}^2 \left[\frac{\nu + \mu d_0}{\wp'(x_i)} \frac{\zeta(x_i)}{\mu} - \frac{K_j}{\wp'(u_{ji})} \frac{\zeta(u_{ji})}{\gamma} \right] \right) \quad (49)$$

and

$$\Gamma = a(L_z - aE) + C_0 + \sum_{i=1}^4 \sum_{j=1}^2 \left[a^2 E \frac{1}{\wp'(\bar{x}_i)} \frac{\zeta(\bar{x}_i)}{\mu} - \frac{C_i}{\wp'(u_{ji})} \frac{\zeta(u_{ji})}{\gamma} \right]. \quad (50)$$

These results differ from that of the standard Kerr space-time by the factor of $1/\beta$ in (49).

As shown in [11] the angular frequencies calculated using Mino time λ are related to the angular frequencies Ω_r , Ω_θ and Ω_ϕ calculated using a distant observer time as follows

$$\Omega_r = \frac{\Upsilon_r}{\Gamma}, \quad \Omega_\theta = \frac{\Upsilon_\theta}{\Gamma}, \quad \Omega_\phi = \frac{\Upsilon_\phi}{\Gamma}. \quad (51)$$

If these frequencies are different they give rise to the precession of the orbital ellipse and of the orbital plane. In particular, the perihelion shift is related to the difference between the angular frequency of the radial motion Ω_r and the angular frequency of the ϕ -motion, while the Lense–Thirring (LT) precession is related to the difference between the frequencies of the two angular motions

$$\Omega_{\text{perihelion}} = \Omega_\phi - \Omega_r \quad , \quad \Omega_{\text{LT}} = \Omega_\phi - \Omega_\theta \quad . \quad (52)$$

In comparison to the standard Kerr space–time with $\beta = 1$, the frequencies of the perihelion shift $\Omega_{\text{perihelion}}$ and the Lense–Thirring precession Ω_{LT} are hence bigger for $\beta < 1$, i.e. in the Kerr space–time including a deficit angle. This is e.g. clearly seen in Fig. 9, where the perihelion shift increases for decreasing β (see plots in the x - y -plane) and the increase of precession is seen when studying the 3-d orbits.

Using the results from the LAGEOS satellites [27] we can estimate an upper bound for the deficit parameter and hence for the energy per unit length of a cosmic string piercing the earth. The theoretical value of the Ω_{LT} for the earth is given by $39 \cdot 10^{-3}$ arcseconds/year. The LAGEOS satellites have measured this value with an accuracy of 10%. Using this we find that

$$\Omega_{\text{LT}}(\beta \neq 1) - \Omega_{\text{LT}}(\beta = 1) = \left(\frac{1}{\beta} - 1\right) \Omega_\phi(\beta = 1) \leq 4 \cdot 10^{-3} \text{arcseconds/year} \quad . \quad (53)$$

Assuming that $\Omega_\phi(\beta = 1)$ is approximately 2π per day, we find that

$$\frac{1}{\beta} - 1 \lesssim 10^{-11} \Rightarrow \frac{\delta}{2\pi} \lesssim 10^{-11} \quad . \quad (54)$$

This transfers to a bound on the energy per unit length μ of a cosmic string piercing the earth that reads

$$\mu \lesssim 10^{16} \text{ kg/m} \quad . \quad (55)$$

Surprisingly, this upper bound is in very good agreement with that found for a cosmic string piercing a Schwarzschild black hole when comparing the theoretical results with the experimental results for the perihelion shift of Mercury and the light deflection by the Sun [19].

VII. CONCLUSIONS

It would be fascinating to detect cosmic strings in the universe since this detection would open the window to the physics of the very early universe and could prove (or disprove) theories such as string theory, supersymmetry and Grand Unification. In most cases the prediction of the detection of these objects has focused on the Cosmic Microwave background (CMB) data [28]. Here we discuss another possibility, namely that cosmic strings might be detected due to the way that test particles move in their space–time. Hence, in this paper we have studied the analytical solutions of the geodesic equation in the space–time of a Kerr black hole pierced by an infinitely thin cosmic string aligned with the rotation axis of the black hole. We have given the analytical solutions for the t -, r -, θ - and ϕ -components of the geodesic equation in terms of Mino time which allows to decouple the r - and θ -motion. We see that the main difference to the standard Kerr space–time (which corresponds to the limit of vanishing deficit angle) is the change of the ϕ -motion. In particular the precession of the orbital plane as well as of the orbital ellipse of bound orbits will increase for increasing deficit angle, i.e. increasing energy per unit length of the string. Comparing our results with the LAGEOS data, we find that the upper limit for the energy per unit length of a cosmic string piercing the earth is $\mu \lesssim 10^{16}$ kg/m. Our results have also applications in the computation of gravitational wave templates for extreme mass ratio inspirals and to the recently suggested alignment of the polarization vector of quasars, respectively.

Acknowledgments The work of PS was supported by DFG grant HA-4426/5-1.

-
- [1] Y. Hagihara, *Theory of relativistic trajectories in a gravitational field of Schwarzschild, Japan. J. Astron. Geophys.* **8**, 67 (1931).
[2] S.Chandrasekhar, *The Mathematical Theory of black holes*, Oxford University Press (1998).
[3] E. Hackmann and C. Lämmerzahl, *Phys. Rev. D* **78** 024035 (2008); *Phys. Rev. Lett.* **100**, 171101 (2008).
[4] E. Hackmann, V. Kagramanova, J. Kunz and C. Lämmerzahl, *Phys. Rev. D* **78** 124018 (2008); [Erratum-ibid. **79** (2009) 029901]

- [5] B. O'Neill, *The Geometry of Kerr black holes*, AK Peters, Massachusetts (1995).
- [6] G. Kraniotis, *Class. Quantum Grav.* **21**, 4743 (2004).
- [7] Y. Mino, *Phys. Rev. D* **67** 084027 (2003).
- [8] R. Fujita and W. Hikida, *Class. Quantum Grav.* **26** 135002 (2009).
- [9] E. Hackmann, V. Kagramanova, J. Kunz and C. Lämmerzahl, *Phys. Rev. D* **81** 044020 (2010); E. Hackmann, C. Lämmerzahl, and A. Macias, *Complete classification of geodesic motion in fast Kerr and Kerr-(anti-)de Sitter spacetimes*, In: *New trends in statistical physics: Festschrift in honour of Leopoldo Garcia-Colin's 80th birthday* (World Scientific, Singapore 2010), to appear.
- [10] E. Hackmann, V. Kagramanova, J. Kunz and C. Lämmerzahl, *Europhys. Lett.* **88**, 30008 (2009).
- [11] S. Drasco and S. Hughes, *Phys. Rev. D* **69**, 044015 (2004).
- [12] see e.g. J. Polchinski, *Introduction to cosmic F- and D-strings*, hep-th/0412244 and reference therein.
- [13] A. Vilenkin and P. Shellard, *Cosmic strings and other topological defects*, Cambridge University Press (1994).
- [14] M. Majumdar and A. Davis, *JHEP* **03**, 056 (2002); S. Sarangi and S. Tye, *Phys. Lett.B* **536**, 185 (2002).
- [15] R. Bach and H. Weyl, *Math. Zeit.* **13**, 134 (1922).
- [16] M. Aryal, L. Ford and A. Vilenkin, *Phys. Rev. D* **34**, 2263 (1986).
- [17] F. Dowker, R. Gregory and J. Traschen, *Phys. Rev. D* **45**, 2762 (1992).
- [18] A. Achucarro, R. Gregory and K. Kuijken, *Phys. Rev. D* **52**, 5729 (1995).
- [19] E. Hackmann, B. Hartmann, C. Lämmerzahl and P. Sirimachan, *Phys. Rev. D* **81** 064016 (2010).
- [20] D. Gal'tsov and E. Masar, *Class. Quantum Grav.* **6**, 1313 (1989).
- [21] N. Ozdemir, *Class. Quant. Grav.* **20** 4409 (2003).
- [22] F. Ozdemir, N. Ozdemir and B. T. Kaynak, *Int. J. Mod. Phys. A* **19** 1549 (2004).
- [23] S. G. Fernandes, G. De A. Marques and V. B. Bezerra, *Class. Quant. Grav.* **23** 7063 (2006).
- [24] R. Poltis and D. Stojkovic, *Can primordial magnetic fields seeded by electroweak strings cause an alignment of quasar axes on cosmological scales?*, arXiv:1004.2704 [astro-ph.CO].
- [25] D. Hutsemekers, R. Cabanac, H. Lamy and D. Sluse, *A & A* **441**, 915H (2005).
- [26] B. Carter, *Phys. Rev.* **174** 1559 (1968).
- [27] see e.g. I. Ciufolini, *Nature* **449** 41 (2007).
- [28] N. Bevis, M. Hindmarsh, M. Kunz and J. Urrestilla, *Phys. Rev. Lett.* **100** 021301 (2008); *Phys. Rev. D* **75** 065015 (2007); for a recent review see C. Ringeval, *Cosmic strings and their induced non-Gaussianities in the cosmic microwave background*, arxiv: 1005.4842 (astro-ph).

VIII. APPENDIX

A. Domain of existence for the θ -motion

In order to find the expressions in (24) and (25) we use the variable $v := \cos^2 \theta$ and rewrite (17) as follows

$$d\lambda = -\frac{dv}{\sqrt{\Theta_v}} \quad (56)$$

with $\Theta_v = -4a^2(E^2 + \varepsilon)v^3 + 4(a^2(E^2 + \varepsilon) - L_z^2 - \mathcal{Q})v^2 + 4\mathcal{Q}v$. For $v \in]0 : 1[$ we assume that two of the zeros merge, i.e. we can then write Θ_v as follows

$$\Theta_v = (v - \xi_1)^2 \xi_2 v \quad (57)$$

where ξ_1 and ξ_2 can be given as functions of L_z , E , ε and \mathcal{Q} . These relations can then be used to give L_z in terms of E .

B. Computation of I_θ

Using the substitutions of section IV B the expression dI_θ reads :

$$dI_\theta = -\frac{L_z dv}{(1-v)\sqrt{(\Theta_v)}} + \frac{aE dv}{\sqrt{\Theta_v}} = \frac{\mu(L_z - aE)dw}{\sqrt{4w^3 - g_2w - g_3}} + \frac{L_z(v + \mu d_0)dw}{(w - d_0)\sqrt{4w^3 - g_2w - g_3}}, \quad (58)$$

where $d_0 = \frac{1-\nu}{\mu}$. Let us define the new variable x and the constant x_0 by using the Weierstrass \wp function :

$$x := \int_\infty^w \frac{dw}{\sqrt{4w^3 - g_2w - g_3}} \quad \text{and} \quad x_0 := \int_\infty^{w_0} \frac{dw}{\sqrt{4w^3 - g_2w - g_3}}, \quad (59)$$

i.e. $w = \wp(x; g_2, g_3)$. With this definition x can be solved as a function of Mino time λ :

$$x - x_0 = \frac{\lambda - \lambda_0}{\mu} . \quad (60)$$

In addition dw can be written as

$$dw = \wp'(x)dx = \pm \sqrt{4\wp^3(x) - g_2\wp(x) - g_3}dx \quad \text{where} \quad \wp' = \frac{d\wp(x; g_2, g_3)}{dx} . \quad (61)$$

Inserting dw into (58) gives :

$$dI_\theta = \mu(L_z - aE)dx + (\nu + \mu d_0) \frac{dx}{\wp(x) - d_0} . \quad (62)$$

The first term in (62) can be integrated easily. For the second term, we can use the formula :

$$\int_{x_0}^x \frac{dx}{\wp(x) - d_0} = \sum_{i=1}^2 \frac{1}{\wp'(x_i)} [(x - x_0)\zeta(x_i) + \ln(\sigma(x - x_i)) - \ln(\sigma(x_0 - x_i))] , \quad (63)$$

where $\wp(x_1) = \wp(x_2) = d_0$. The simple poles of the function in (63) denoted by x_1, x_2 are in the fundamental domain $\{2a\omega_1 + 2b\omega_2 | a, b \in [0, 1]\}$, where $2\omega_1 \in \mathbb{R}$ and $2\omega_2 \in \mathbb{C}$. Hence the analytical solution of I_θ is :

$$\begin{aligned} \int dI_\theta = I_\theta &= \mu(L_z - aE)(x - x_0) + \sum_{i=1}^2 \frac{\nu + \mu d_0}{\wp'(x_i)} [(x - x_0)\zeta(x_i) + \ln(\sigma(x - x_i)) - \ln(\sigma(x_0 - x_i))] \\ &= (L_z - aE)(\lambda - \lambda_0) + \sum_{i=1}^2 \frac{\nu + \mu d_0}{\wp'(x_i)} \left[\frac{(\lambda - \lambda_0)}{\mu} \zeta(x_i) + \ln(\sigma(x - x_i)) - \ln(\sigma(x_0 - x_i)) \right] . \end{aligned} \quad (64)$$

C. Computation of I_r

With the substitution $r = \frac{1}{y} + r_1$ the expression dI_r can be written as a function of y as follows :

$$dI_r = \frac{aP(r)dr}{\Delta\sqrt{R(r)}} = - \left(\frac{a}{r_1^2 + a^2 - 2Mr_1} \right) \left[\frac{(Er_1^2 + Ea^2 - L_z a)y^2 + 2Er_1y + E}{y^2 + \frac{2r_1 - 2M}{r_1^2 + a^2 - 2Mr_1}y + \frac{1}{r_1^2 + a^2 - 2Mr_1}} \right] \frac{dy}{\sqrt{R_y}} . \quad (65)$$

Moreover the integral in (65) can be written in the form :

$$dI_r = \left[K_0 + \frac{K_1}{y - y_1} + \frac{K_2}{y - y_2} \right] \frac{dy}{\sqrt{R_y}} , \quad (66)$$

where

$$y_{1,2} = \frac{r_1 - M \pm \sqrt{M^2 - a^2}}{-r_1^2 - a^2 + 2Mr_1} \quad (67)$$

and the $K_i, i = 0, 1, 2$ are constants. Using the transformation $y = \gamma z + \alpha$ (where γ and α are constants) the expression dI_r becomes :

$$dI_r = K_0 \frac{\gamma dz}{\sqrt{4z^3 - \tilde{g}_2 z - \tilde{g}_3}} + \sum_{j=1}^2 K_j \frac{dz}{(z - e_j) \sqrt{4z^3 - \tilde{g}_2 z - \tilde{g}_3}} \quad \text{where} \quad e_j := \frac{y_j - \alpha}{\gamma} \quad (68)$$

We introduce the new variable u as follows :

$$u := \int_\infty^z \frac{dz}{\sqrt{4z^3 - \tilde{g}_2 z - \tilde{g}_3}} , \quad (69)$$

i.e. $\wp(u; \tilde{g}_2, \tilde{g}_3) = z$. Then u can be given as a function of Mino time λ . Finally using (62)-(63) the analytical solution of I_r is :

$$\begin{aligned} \int dI_r = I_r &= \gamma K_0(u - u_0) + \sum_{i,j=1}^2 \frac{K_j}{\wp'(u_{ji})} [(u - u_0)\zeta(u_{ji}) + \ln(\sigma(u - u_{ji})) - \ln(\sigma(u_0 - u_{ji}))] \\ &= -K_0(\lambda - \lambda_0) + \sum_{i,j=1}^2 \frac{K_j}{\wp'(u_{ji})} \left[\frac{-(\lambda - \lambda_0)}{\gamma} \zeta(u_{ji}) + \ln(\sigma(u - u_{ji})) - \ln(\sigma(u_0 - u_{ji})) \right], \quad (70) \end{aligned}$$

where $u = -\left(\frac{1}{\gamma}(\lambda - \lambda_0) + C_r\right)$, $u_0 = -C_r$ and $u_{ji} = e_j$ with $\wp(u_{11}) = \wp(u_{12}) = e_1$ and $\wp(u_{21}) = \wp(u_{22}) = e_2$.

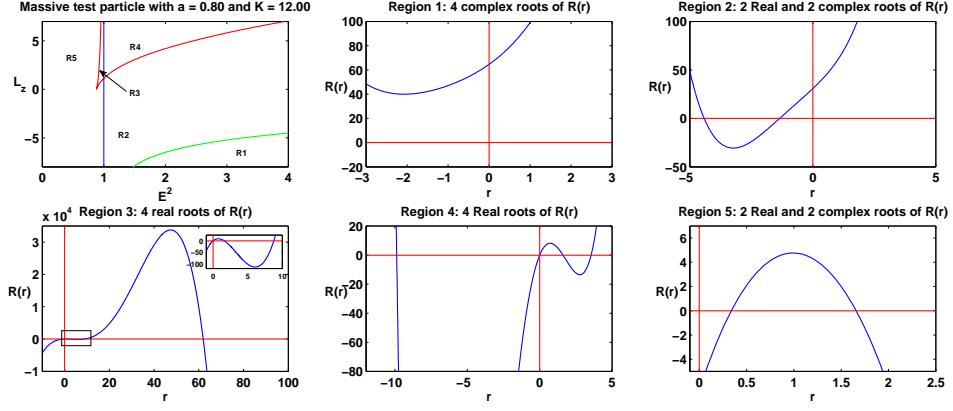
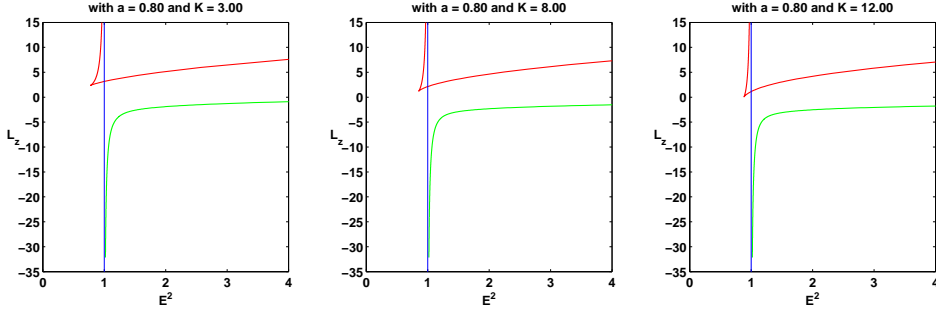
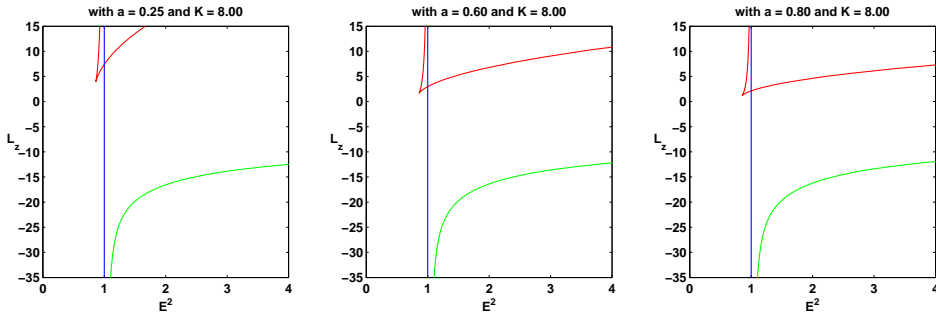


FIG. 1: The domain of existence of solutions to the geodesic equations for $M = 1$, $a = 0.8$ and $K = 4$ that follows from the requirement $R(r) > 0$. The top left figure shows the domain of existence in the L_z - E^2 -plane. The green and red lines represent $R(r) = 0$, where the green line is for $\kappa \in]-\infty : 0]$ and the red line for $\kappa \in [0 : +\infty[$. The remaining figures show the function $R(r)$ for the different domains denoted by R1 to R5.



(a) varying Carter constant K for $M = 1$, $a = 0.8$.



(b) varying a for $M = 1$, $K = 3.0$.

FIG. 2: The change of the L_z - E^2 plot for varying Carter constant (a) and angular momentum per unit mass of the black hole a (b), respectively.

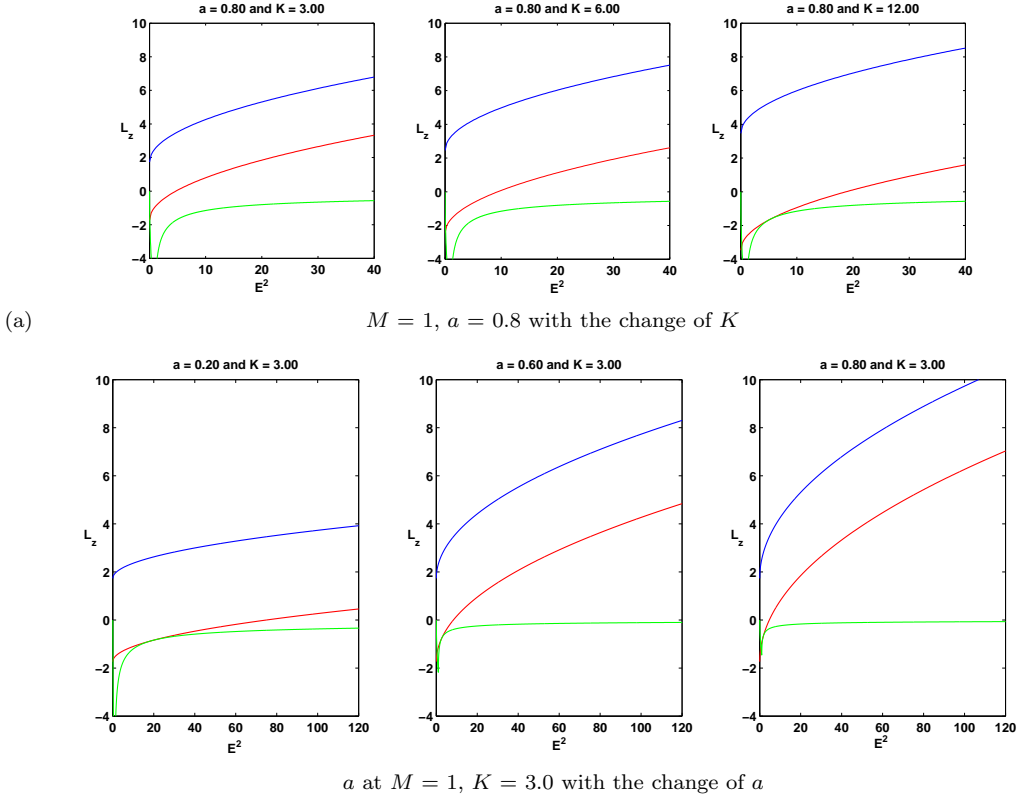


FIG. 3: The change of the domain of existence of solutions to the geodesic equations in the L_z - E^2 plane for several values of the Carter constant K and $M = 1, a = 0.8$ (a) and several values of the angular momentum per unit mass of the black hole a and $M = 1$ and $K = 3$ (b), respectively. Note that solutions exist only below the blue, above the red and above the green line.

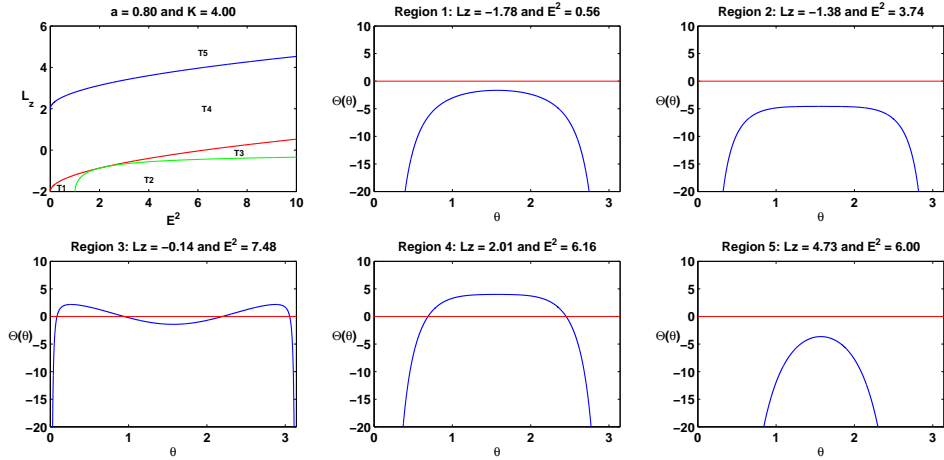


FIG. 4: The domain of existence of solutions to the geodesic equations for $M = 1, a = 0.8$ and $K = 4$ that follows from the requirement $\Theta(\theta) > 0$. The top left figure shows the domain of existence in the L_z - E^2 -plane. The remaining figures show the function $\Theta(\theta)$ for the different domains denoted by $T1$ to $T5$. Solutions exist only for parameters L_z and E in domains $T3$ and $T4$, respectively.

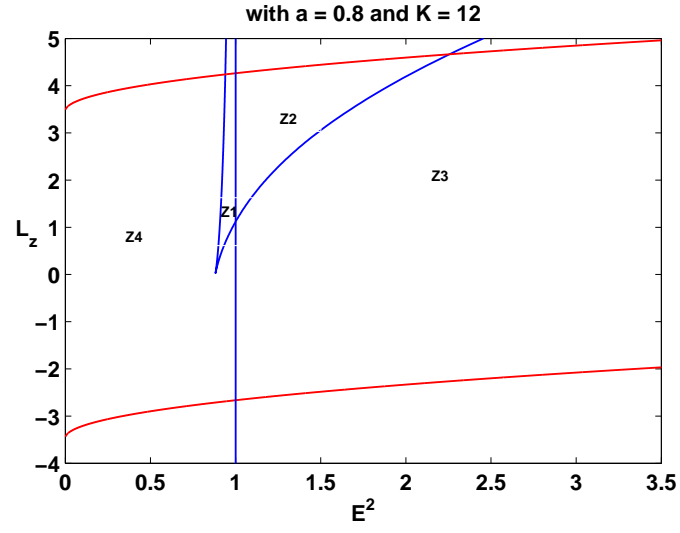


FIG. 5: The four domains Z_1 to Z_4 in the L_z - E^2 -plane for which solutions to the geodesic equation for massive particles exist are shown for $M = 1$, $a = 0.8$ and $K = 12$. The red and blue lines come from the restriction $\Theta(\theta) > 0$ and $R(r) > 0$, respectively.

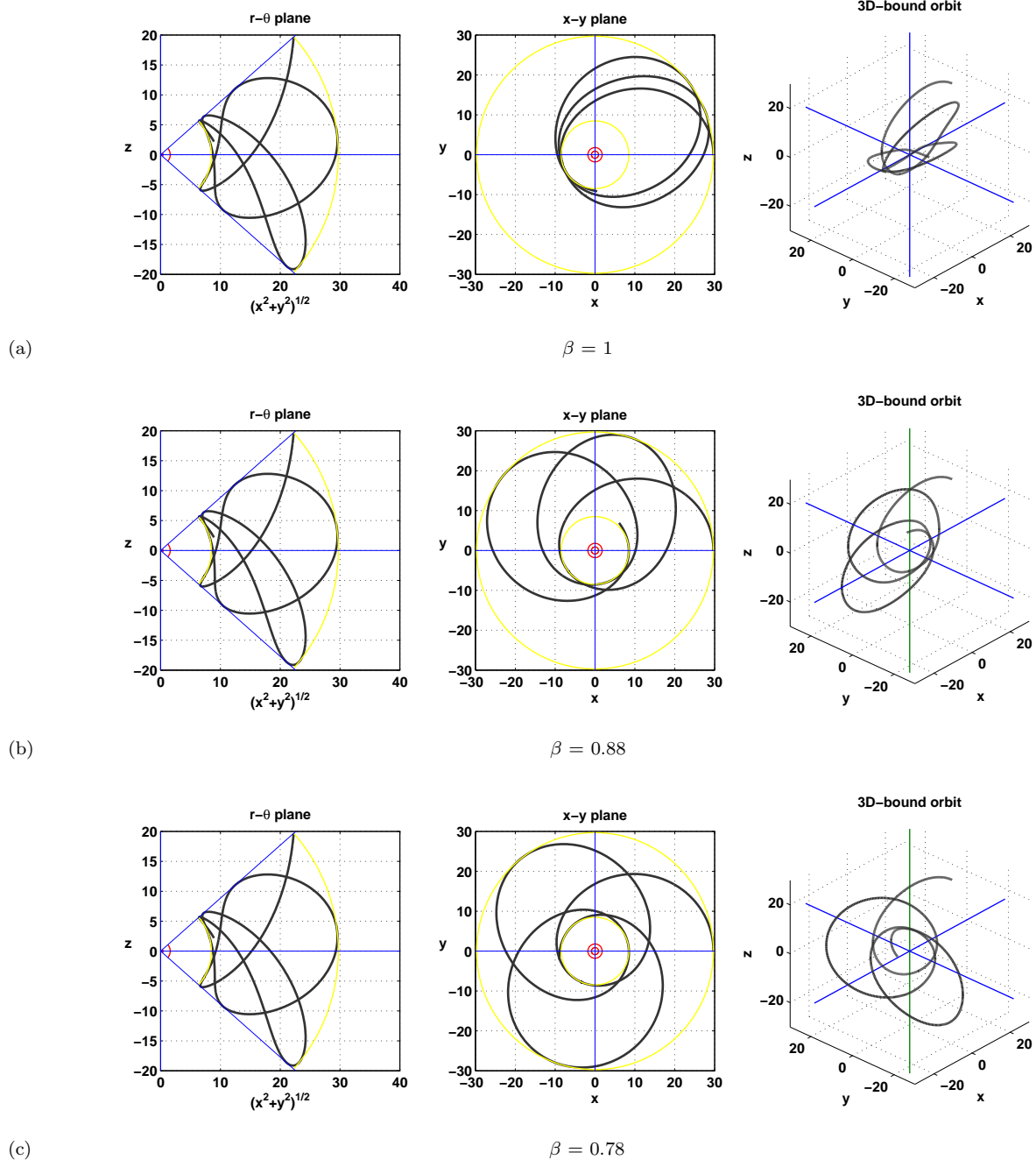


FIG. 6: The change of the outer bound orbit of a massive test particle (domain Z1) due to the change of the deficit parameter β . Here $L_z = 3.0$, $E = \sqrt{0.95}$, $K = 12$, $M = 1$ and $a = 0.8$. The red circles represent the radii of the event and Cauchy horizons, while the yellow circles denote the minimal and the maximal radius of the orbit, respectively.

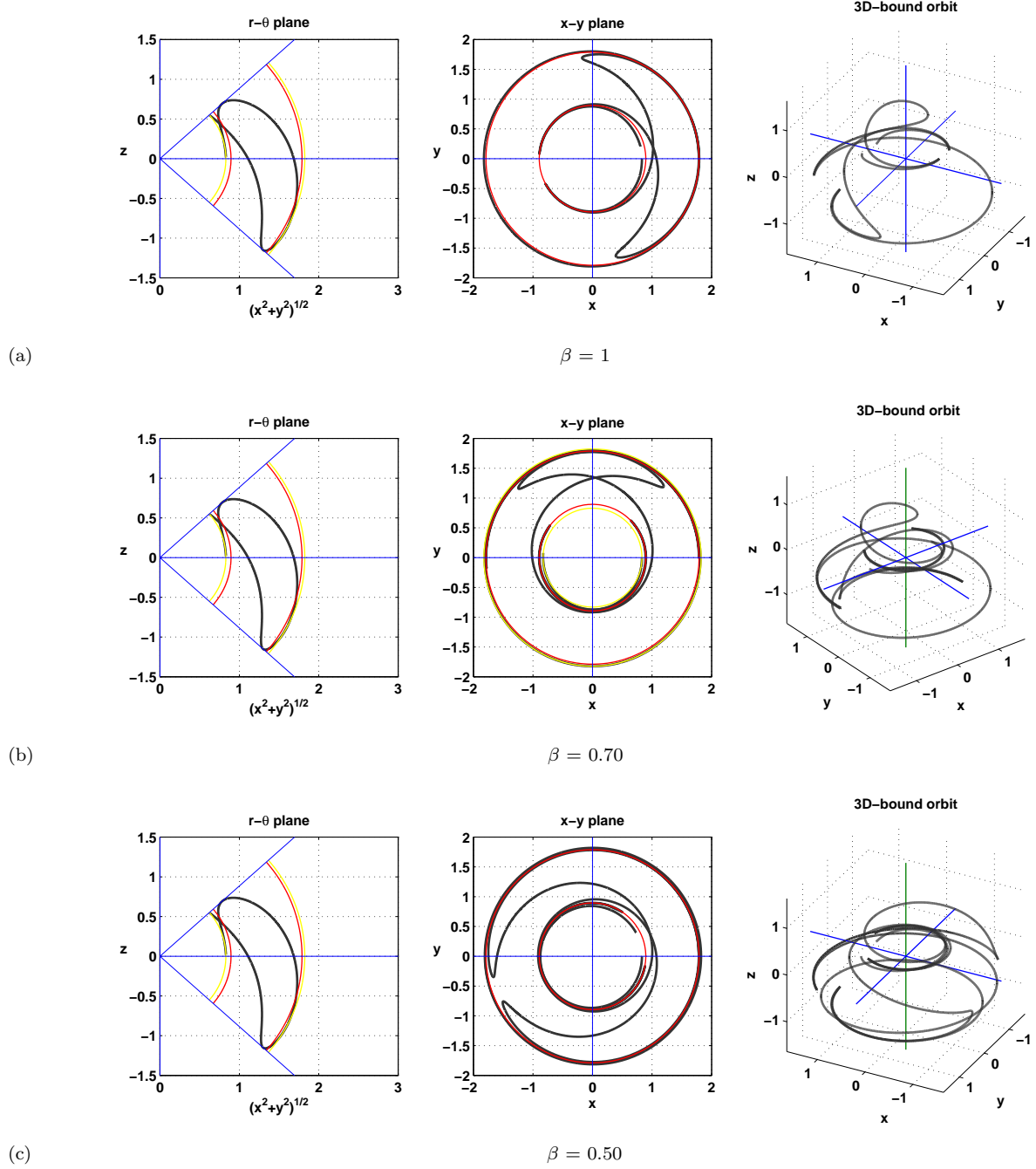


FIG. 7: The change of the inner bound orbit of a massive test particle (domain Z1) due to the change of the deficit parameter β . Here $L_z = 3.0$, $E = \sqrt{0.95}$, $K = 12$, $M = 1$ and $a = 0.8$. The red circles represent the radii of the event and Cauchy horizons, while the yellow circles denote the minimal and the maximal radius of the orbit, respectively.

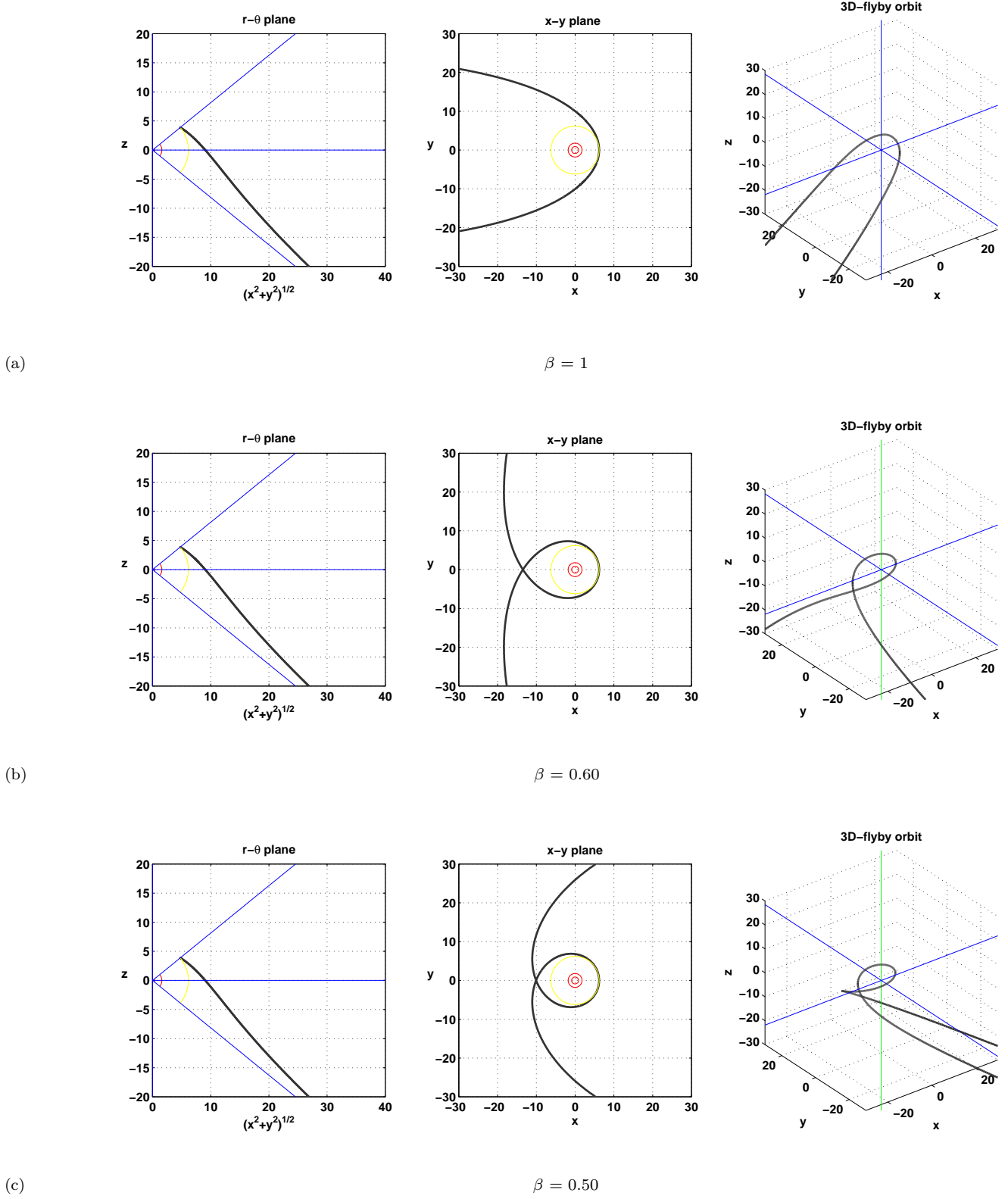


FIG. 8: The change of the flyby orbit (domain Z2) of a massive test particle due to the change of the deficit parameter β . Here $L_z = 3.104$, $E = 1.004$, $K = 12$, $M = 1$ and $a = 0.8$. The red circles represent the radii of the event and Cauchy horizons, while the yellow circle denotes the minimal radius of the orbit.

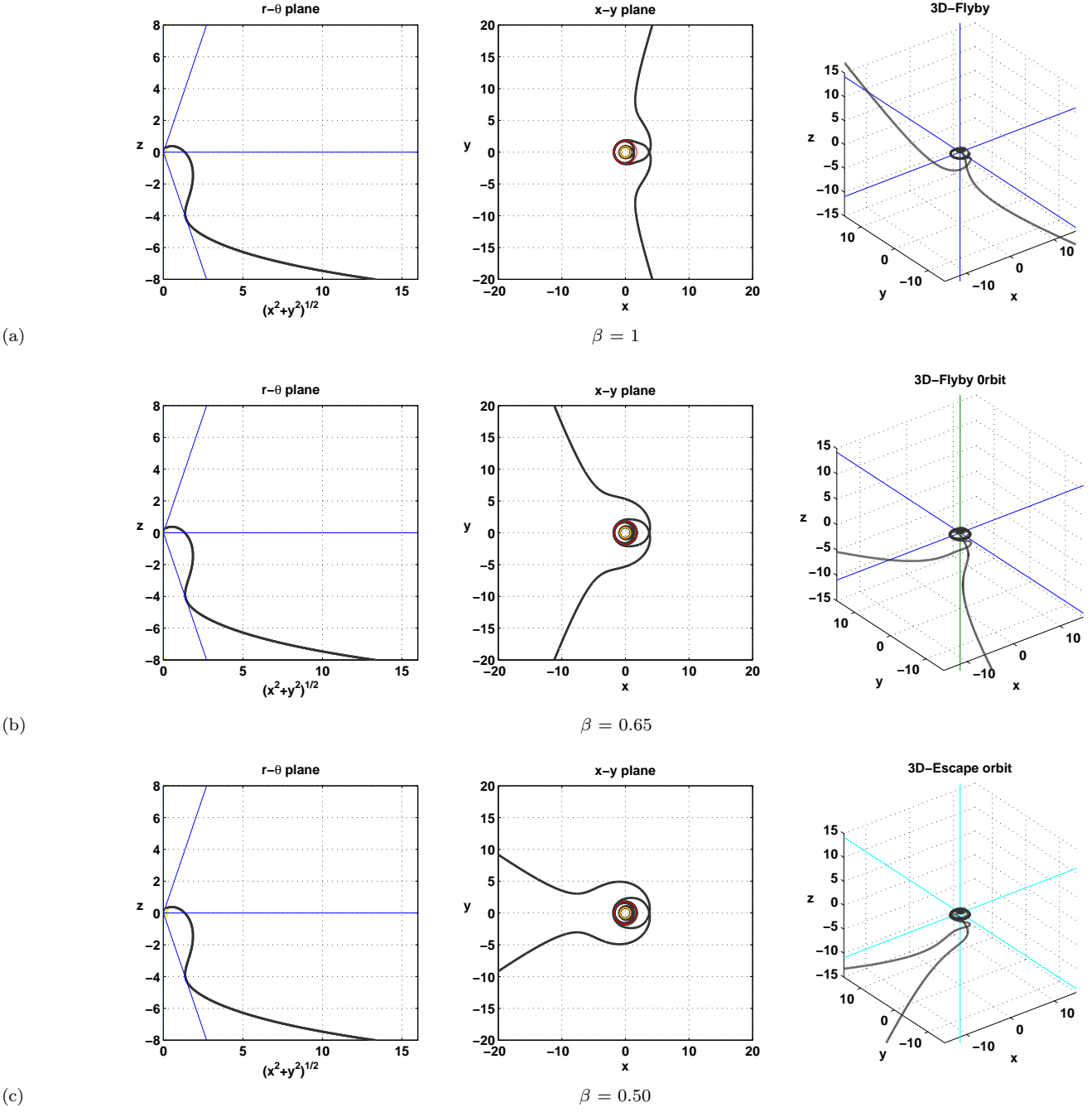


FIG. 9: The change of the flyby orbit (domain Z3) of a massive test particle due to the change of the deficit parameter β . Here $L_z = -1$, $E = \sqrt{1.10}$, $K = 12$, $M = 1$ and $a = 0.8$. The red circles represent the radii of the event and Cauchy horizons, while the yellow circle denotes the minimal radius of the orbit.

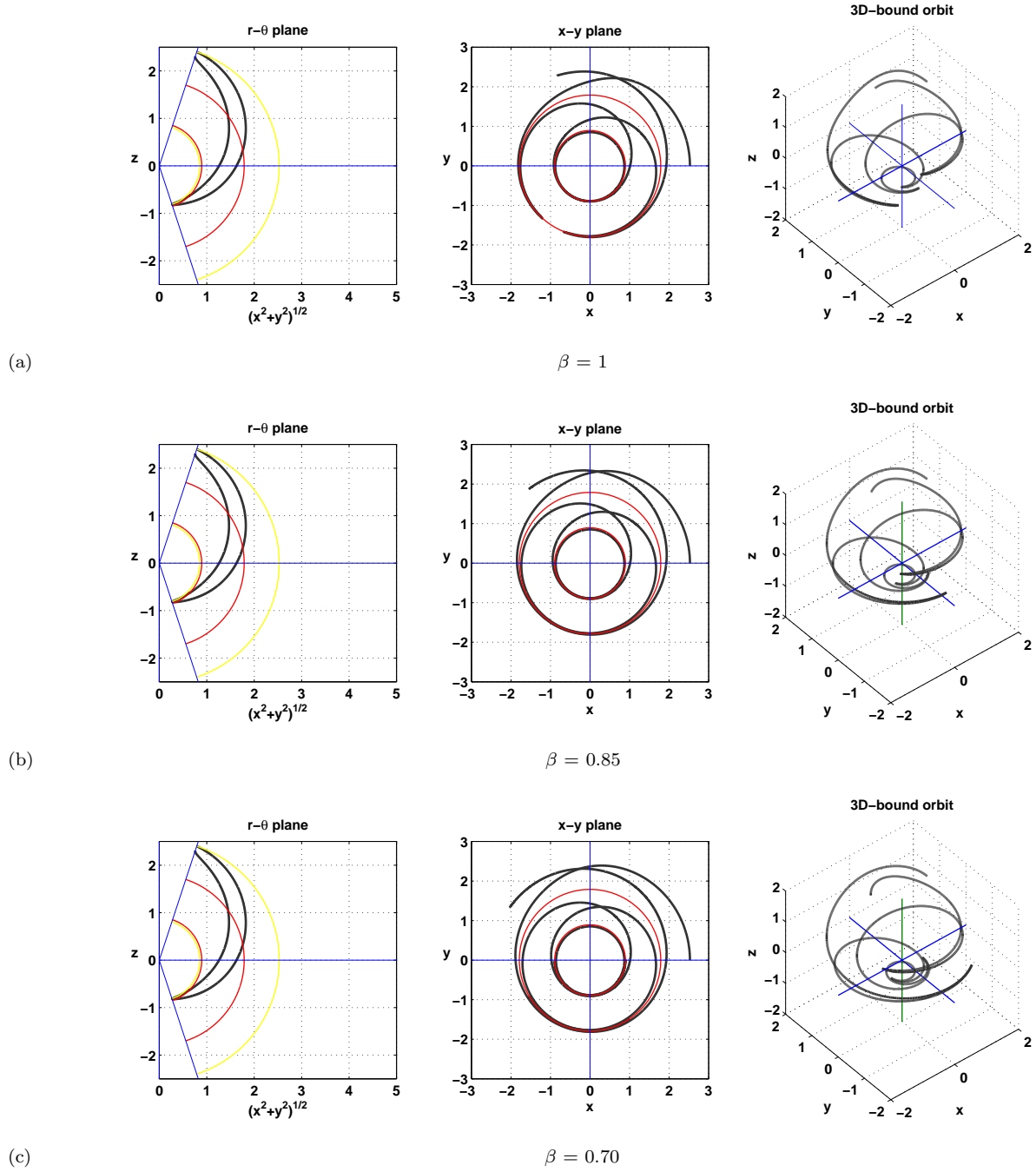


FIG. 10: The change of the bound orbit (domain Z4) of a massive test particle due to the change of the deficit parameter β . Here $L_z = -1$, $E = \sqrt{0.5}$, $K = 12$, $M = 1$ and $a = 0.8$. The red circles represent the radii of the event and Cauchy horizons, while the yellow circles denote the minimal and maximal radius of the orbit, respectively.

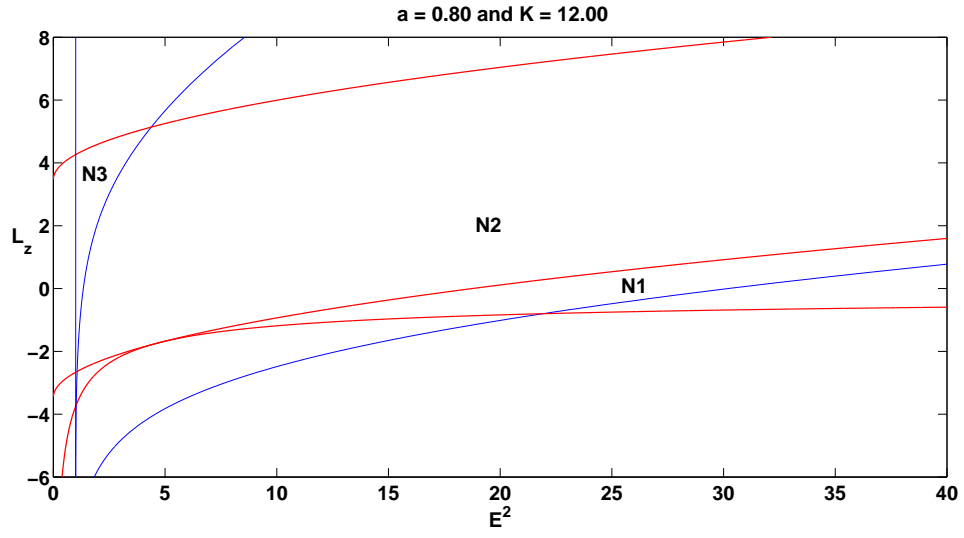


FIG. 11: The three domains N1 to N3 in the L_z - E^2 -plane for which solutions to the geodesic equation for massless particles exist are shown for $M = 1$, $a = 0.8$ and $K = 12$. The red and blue lines come from the restriction $\Theta(\theta) > 0$ and $R(r) > 0$, respectively.

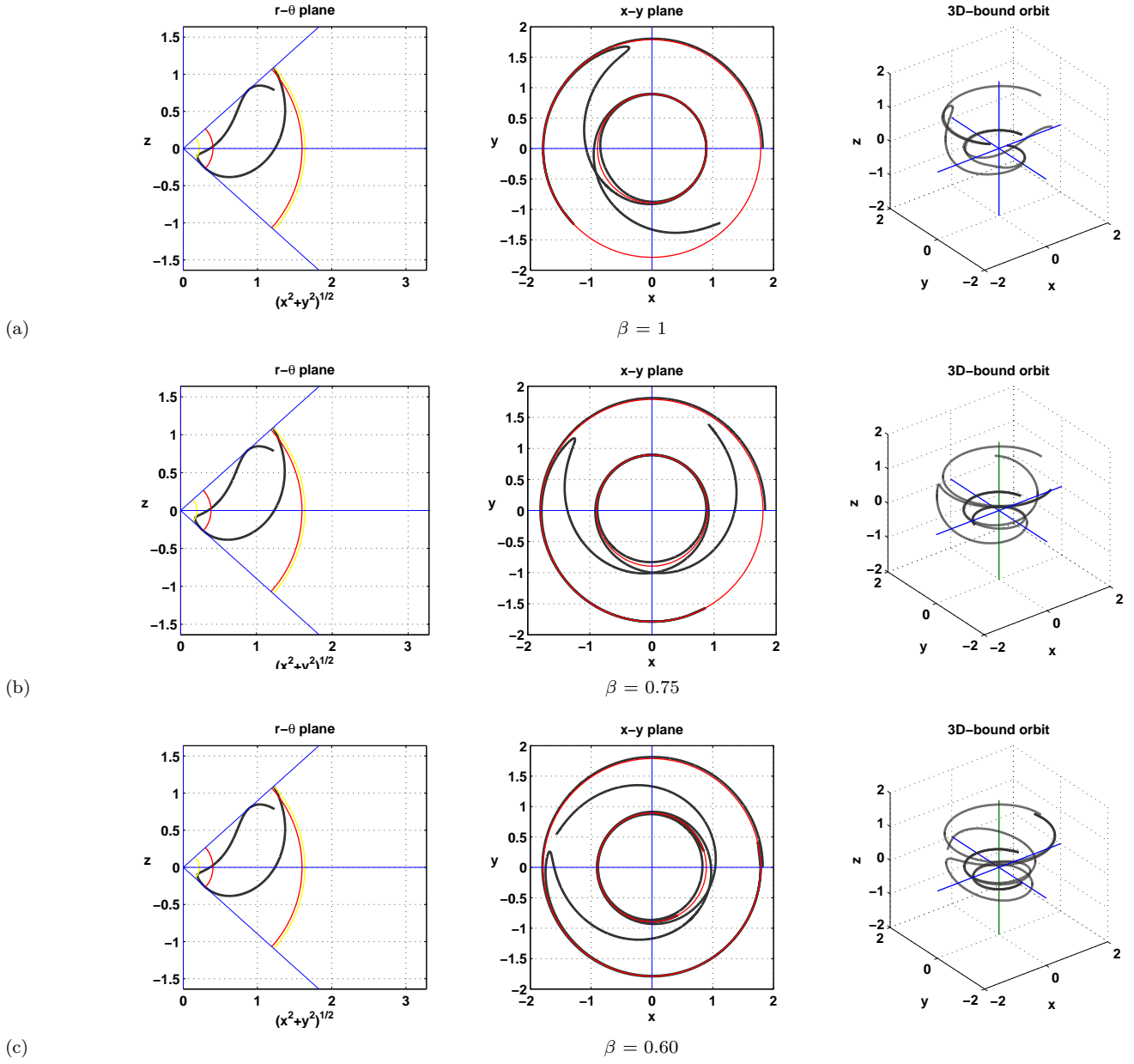


FIG. 12: The change of the bound orbit (domain N3) of a massless test particle due to the change of the deficit parameter β . Here $L_z = 3.0$, $E = \sqrt{0.90}$, $K = 12$, $M = 1$ and $a = 0.8$. The red circles represent the radii of the event and Cauchy horizons, while the yellow circles denote the minimal and maximal radius of the orbit, respectively.

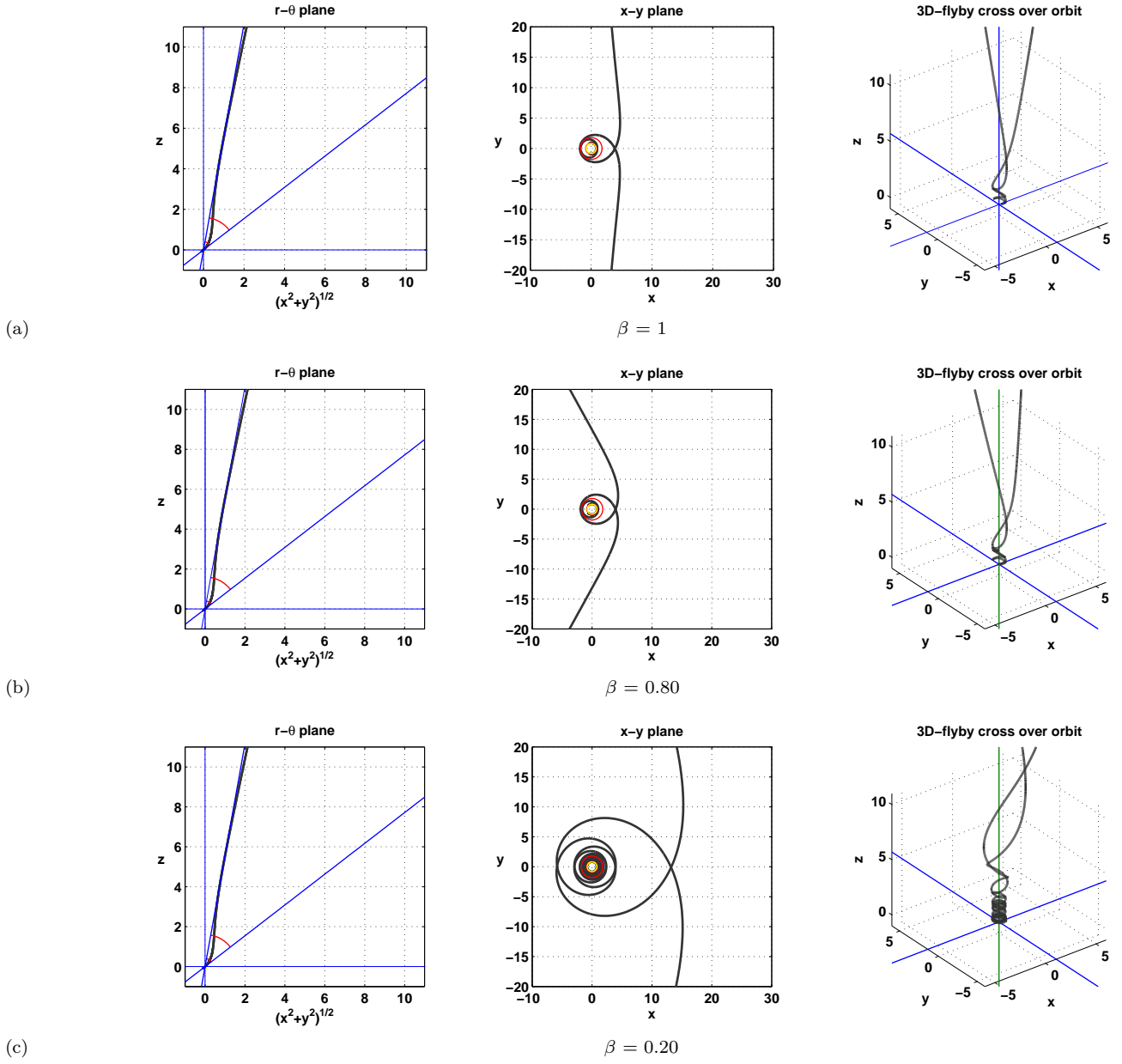


FIG. 13: The change of the cross-over flyby orbit (domain N1) of a massless test particle due to the change of the deficit parameter β . Here $L_z = -0.50$, $E = \sqrt{20}$, $K = 12$, $M = 1$ and $a = 0.8$. The red circles represent the radii of the event and Cauchy horizons, while the yellow circle denotes the minimal radius of the orbit.

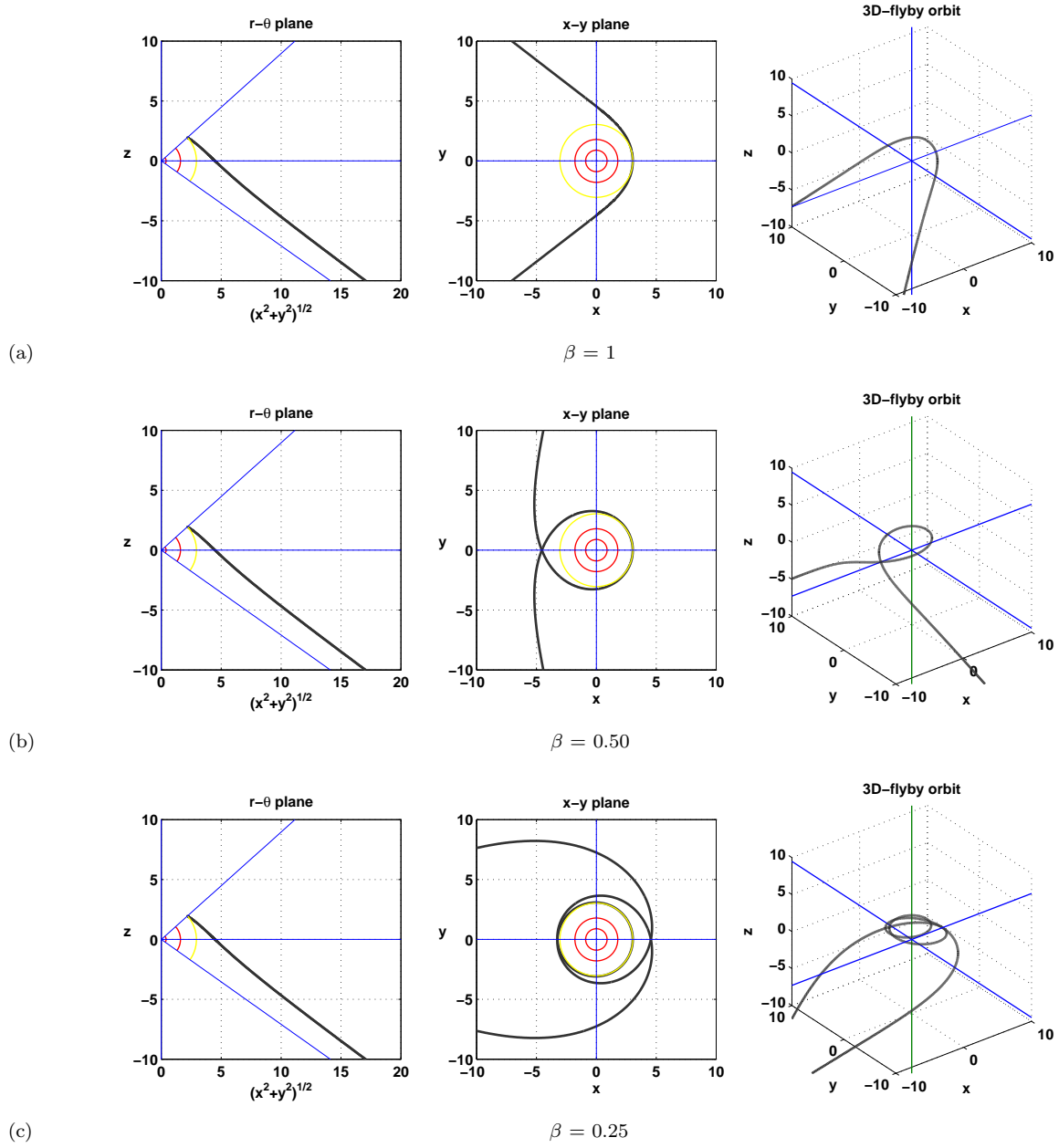


FIG. 14: The change of the flyby orbit (domain N3) of a massless test particle due to the change of the deficit parameter β . Here $L_z = 3$, $E = \sqrt{0.9}$, $K = 12$, $M = 1$ and $a = 0.8$. The red circles represent the radii of the event and Cauchy horizons, while the yellow circle denotes the minimal radius of the orbit.